Received: 15 January 2022 | Revised: 20 February 2022 | Accepted: 22 March 2022

DOI: 10.1002/pat.5680

RESEARCH ARTICLE

polymers advanced technologies WILEY

Surface modification of graphene oxide for preparing self-healing nanocomposite hydrogels

Ezgi B. Çeper | Esra Su | Oguz Okay | Orhan Güney

Departments of Chemistry and Polymer Science & Technology, Istanbul Technical University, Istanbul, Turkey

Correspondence
Oguz Okay and Orhan Güney, Departments of Chemistry and Polymer Science & Technology, Istanbul Technical University, Maslak, 34469 Istanbul, Turkey.
Email: okayo@itu.edu.tr and oguney@itu.edu.tr

Funding information
Istanbul Technical University, Grant/Award Number: 42666

Abstract

In this work, graphene oxide (GO) and vinyl modified GO (V-GO)-based nanocomposite hydrogels with improved mechanical property and self-healing ability have been synthesized and characterized. GO first was synthesized by modified Hummer's method using graphite powder and then functionalized with vinyl groups by using (3-mercaptopropyl) trimethoxysilane (MPTS) via silanization method. The GO and V-GO nanoparticles were characterized by FT-IR, UV–vis spectroscopy, SEM, and dynamic light scattering technique (DLS). Hydrogels were obtained by in-situ free-radical polymerizations of acrylamide (AAm) and [3-(methacryloylamino)propyl] trimethylammonium chloride (MAPTAC) monomers in the presence of GO and V-GO nanoparticles. The effects of the amount of GO and V-GO on the gelation profile and viscoelastic characteristics of the hydrogels were studied. The pH-responsive action, swelling behavior, and swelling kinetics of the hydrogels with various GO and V-GO contents were also evaluated. The mechanical performance of nanocomposite cationic hydrogels prepared with GO and V-GO nanosheets was compared to the neat AAm-MAPTAC hydrogels. The self-healing ability of the hydrogels were elucidated as a function of the amount of GO and V-GO nanosheets bound to the polymer network by physical interactions and chemical cross-links, respectively.

KEYWORDS
mechanical properties, modified graphene oxide, nanocomposite hydrogels, self-healing

1 | INTRODUCTION

Among various attractive properties of hydrogels, outstanding attention was paid in the past decade to incorporate self-healing behavior into the hydrogel network which would further expand their application areas. The self-healing function is originated from living organisms and tissues where the crack or damage is restored autonomously.[1] Derived from this natural phenomenon, several techniques have been developed for preparing self-healing hydrogels that heal themselves autonomously or under the effect of a stimulus to recovery their initial properties after damage. This smart function leads to an enhanced lifetime of the synthetic materials, and provides cost efficiency.[2,3] Up to date, there are different strategies proposed to achieve healing behavior in hydrogels, such as integrating healing agents, reversible noncovalent bonds, for example, hydrophobic interactions,[4,5] hydrogen bonding,[6,7] metal–ligand coordination,[8,9] $\pi - \pi$ stacking[10,11] and ionic bonding,[12,13] and dynamic covalent bond formations including disulfide bonds,[14] imine bonds,[15] Diel-Alder (DA) "click chemistry,"[16] acylhydrazone bonds,[17] boronate-catechol complexation,[18] and some dynamic reshuffling radical reactions.[19,20]

Even tough hydrogels have many advantageous, they usually tend to show low mechanical strength which limits their load bearing and strength required applications.[21] Great efforts have been offered to develop both mechanically strong and self-healable hydrogels. The strategies to enhance the strength of hydrogels include double and triple network hydrogels,[22,23] topological "slide-ring" hydrogels,[24,25] and incorporation of clays and nanoparticles into polymer networks.[26–28]

Due to the superior thermal and electronic properties, graphene oxide (GO) based nanoparticles have been attracted significant attention.[29,30] Owing to their high surface activity, excellent mechanical strength, abundant polar functional groups, and processability, GO nanoparticles have been incorporated into hydrogel networks.[31–33] GO has a large amount of hydrophilic oxygenated functional groups on its surface such as epoxide, carboxylic acid, hydroxyl, which enable GO to be modified by covalent and noncovalent methods for further opportunities.[34,35] GO has been studied as a filler to increase the thermal and mechanical properties of various nanocomposite polymer networks either by simple physically mixing the nanoparticles in solutions,[36,37] or by in situ polymerization of the monomer and cross-linker in the presence of GO.[38] GO-based nanocomposite gels exhibit enhanced mechanical properties and also demonstrate self-healing behavior without the presence of healing agents.[39–41]

Additionally, high specific surface area and large amount of functional groups on the surface of GO nanoparticles make GO-containing hydrogels a significant candidate to be used in applications for ion and dye adsorptions,[42,43] water treatments,[44,45] drug delivery systems,[46,47] sensors and actuators,[48,49] and tissue engineering.[50,51] Shen et al. have synthesized GO based poly (acrylic acid) (PAA) hydrogels to investigate their thermal, mechanical and swelling properties. After incorporation of GO into the hydrogel network, the resulted hydrogels show a high toughness and good mechanical strength together with an elongation at break of four times higher than that of neat PAA.[52] Pan et al. have synthesized cationic GO based polyacrylamide hydrogels through free-radical polymerization of 2-(dimethylamino)ethyl acrylate methochloride (DAC) and acrylamide (AAm) in the presence of GO. Due to the ionic interactions between GO and DAC, and hydrogen bonding interactions between GO and AAm providing an energy dissipating mechanism, the resulting hydrogels show self-healing behavior with an efficiency of above 92% with respect to the tensile strength, tensile strain, and toughness.[53]

Although GO as a nano-filler is effective for the improvement of mechanical properties of composite materials, their physical entrapment inside the gel network diminishes the reusability of hydrogels for many applications due to the release of nanosheets from the matrix upon swelling-deswelling cycles in solution. Therefore, the aim of this study was to figure out the conditions that provide entrapment of GO nanosheets in the hydrogel network via covalent rather than physical bonds. To achieve this main goal, GO surfaces were functionalized with vinyl groups using (3-Mercaptopropyl) trimethoxysilane (MPTS) via silanization method. To investigate the effect of vinyl-modified GO (V-GO) on hydrogel properties, free-radical polymerization of acrylamide (AAm) and [3-(Methacryloylamino)propyl] trimethylammonium chloride (MAPTAC) monomers was conducted in the presence of V-GO nanoparticles. The swelling, viscoelastic, and mechanical characteristics as well as the self-healing behavior of AAm-MAPTAC hydrogels containing V-GO were determined and compared with the neat and GO-containing hydrogels.

2 | EXPERIMENTAL PART

2.1 | Materials

Acrylamide (AAm), [3-(methacryloylamino)propyl] trimethylammonium chloride (MAPTAC) in aqueous solution (50%), *N*,*N*′-methylenebis (acrylamide) (BIS), [3-(methacryloyloxy) propyl] trimethoxysilane (MPTS), 2,2′-azobis(2-methylpropionamidine) dihydrochloride (AIBA), sodium hydroxymethanesulfinate dihydrate (ALD), and ammonium persulfate (APS) were supplied from Sigma Aldrich Co. Graphite powder (99.9%, 5–10 μm) was provided from NANOGRAFI company (Ankara, Turkey). Sodium nitrate ($NaNO_3$), sulfuric acid (H_2SO_4), potassium permanganate ($KMnO_4$), hydrogen peroxide (H_2O_2), ethanol and the other chemicals were supplied from Merck.

2.2 | Apparatus

Agilent Cary 630 FTIR spectrometer was used to record the attenuated total reflectance-infrared (ATR-FTIR) spectra of the samples. VWR pH-Meter 730P equipped with a combined glass electrode was utilized to measure the pH of the solutions. The field emission scanning electron microscopy (FE-SEM) images used for characterizing the surface morphology of as-prepared GO and V-GO nanoparticles were acquired on a Zeiss Sigma 300 microscope with a tungsten filament at an accelerating voltage of 200 V–30 kV. Size distributions and zeta potentials of the particles were determined using dynamic light scattering technique (DLS) on a Zetasizer Nano-ZSP instrument (Malvern Instruments Ltd, UK) using a standard rectangular quartz cell. UV–vis spectrometer (Ocean Optics USB 2000 with CCD array detector) was used for recording the spectra of GO and V-GO nanoparticles dispersed in aqueous solution. Thermogravimetric analysis (TGA) was performed to gain additional knowledge on proof of modification and thermal stability of GO upon silanization processes. The nanoparticle samples (5–10 mg) were positioned in platinum pans and characterized by using a Perkin-Elmer Diamond TA/TGA applying a heating rate of 10°C/min under nitrogen gas.

2.3 | Production of GO and V-GO

Graphene oxide (GO) was produced from graphite powder by a modified Hummer's method as shown in Figure 1. Briefly, 0.5 g of graphite was added into a 250 ml flask immersed in an ice-water bath. After addition of $NaNO_3$ (0.5 g) and concentrated H_2SO_4 (23 ml) under stirring, the solution was stirred for 20 min. Then, 3 gr of $KMnO_4$ was added stepwise under stirring and the mixture was kept at 35°C for 2 h. Thereafter 140 ml of de-ionized water was poured into the mixture and the temperature was then elevated to 90°C. Lastly, 3 ml of H_2O_2 (35%) was added slowly until the color of the solution turned brilliant yellow. After centrifugation, the final product was washed with a dilute hydrochloric acid solution to extract the excess ions and

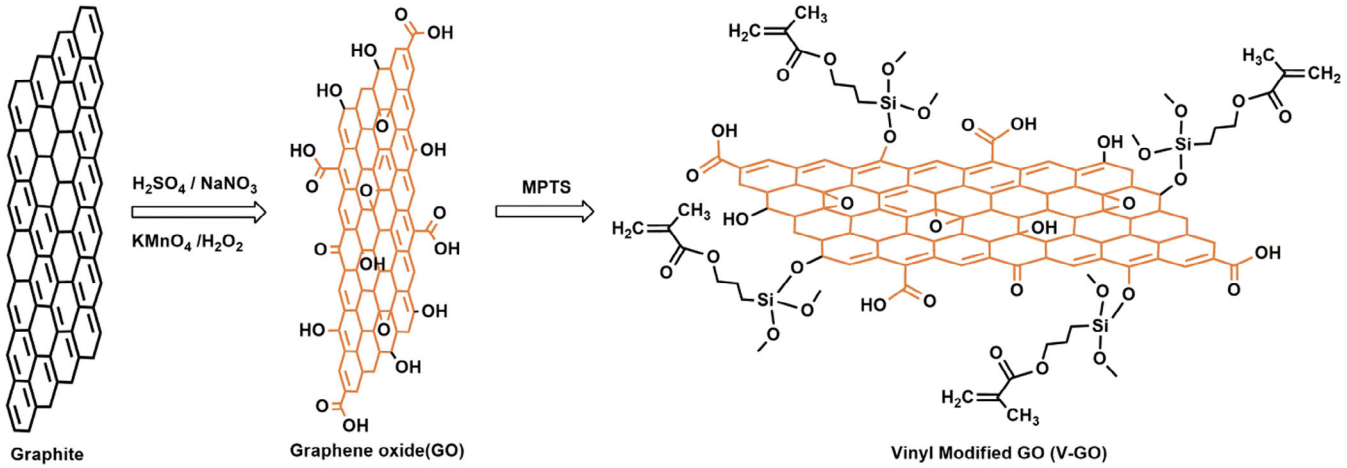

FIGURE 1 Synthesis of GO from graphite and silanization of GO for the synthesis of V-GO

then rinsed with deionized water to extract the acid. The product was then dried at 55°C under vacuum for the production of GO powder.

The functionalization of the GO surfaces with vinyl groups to produce vinyl modified GO (V-GO) was carried out by reacting GO with 3-methacryloxypropyltrimethoxysilane molecule (MPTS) as shown in Figure 1. Briefly, about 200 mg of GO powder was added into a 500 ml flask containing 150 ml of ethanol, and dispersed by ultrasonication for 30 min. 1200 µl of MPTS was then added into the flask under vigorous stirring at 55°C. The flask was kept in a water bath at 55°C for 24 h. After the process was terminated, the flask was cooled down to room temperature. The product separated by centrifugation was washed with water two times and then dried at 50°C under vacuum. V–GO thus obtained as dark brown powder was stored for further applications.

Although aqueous dispersions of GO can easily be prepared because of its hydrophilic nature, the silanization of GO to produce V-GO could alter the dispersion stability since oxidizing procedure is proceeded through functional hydrophilic groups of GO.[54] Therefore, before the synthesis of nanocomposite hydrogels, the stability of aqueous suspensions of both GO and V-GO depending on pH was investigated. Lower pH values resulted in inhomogeneous suspensions due to the flocculation behavior of GO and V-GO while stable dispersions were obtained at pH = 10. Moreover, the change in pH or nanoparticle concentration resulted in color changes of the nanoparticle dispersions (Figures S1 and S2). With an increase in the pH value, or nanoparticle concentration, the solution gradually turns darker and becomes slightly clear at pH 10 which demonstrates a better dispersion of GO and V-GO nanosheets.

2.4 | Preparation of nanocomposite hydrogels

AAm-MAPTAC/GO nanocomposite hydrogels were synthesized by in-situ free-radical copolymerization of MAPTAC and AAm in the presence of GO. Typically, to prepare hydrogels at a GO concentration of 1 mg ml^{-1}, 10 mg of GO powder was dispersed in 10 ml of water by ultrasonication for about 1 h and then kept under stirring for 24 h before usage. The pH of the GO dispersion was then adjusted to pH 10 by dropping ammonia solution (6% in aqueous solution), and the mixture was stirred for about 20 min under ice water bath. Then, 4.4 g of MAPTAC, 1.4 g of AAm, and 400 µl of a BIS stock solution (12 mg ml^{-1}) were added to the GO solution following another 1 h of stirring to make a uniform solution under ice bath. Finally, 256 µl of APS (62.5 mg ml^{-1}), 192 µl AIBA (0.12 g ml^{-1}) and 192 µl of ALD (0.12 g ml^{-1}) were added to the mixture and stirred for about 5 minutes. After 2 min of ultrasonication, the mixtures were transferred to the cylinder molds with an inner diameter of 4.6 mm. Polymerization was conducted in a thermostatic water bath at 35°C for 24 h. The resulting hydrogel was removed from the tube and stored for further characterization (Figure 2).

AAm-MAPTAC/V-GO nanocomposite hydrogels were prepared as above except that V-GO was used instead of GO (Figure 2). To elucidate the effect of the nanoparticles on the hydrogel properties, four different concentrations of GO and V-GO suspensions (1, 2, 4, and 6 mg ml^{-1}) were used in the hydrogel preparation. Additionally, neat AAm-MAPTAC hydrogel was also prepared for comparison.

2.5 | Swelling measurements and gel fraction

Nanocomposite hydrogel specimens were cut in a cylindrical form with a diameter of 4.6 mm and 5.0 mm in length, and placed in oven at 60°C for about 24 h. The dried specimens were weighted and immersed into distilled water with various pH at 23°C for about 3 days. The pH of the solution was adjusted to pH 3.0 and 12.0 by dropping hydrochloric acid and sodium hydroxide solutions, respectively. The mass (m) of hydrogels was recorded depending on time. The relative mass, m_{rel} of the specimens was computed as:

$$m_{rel} = \frac{m}{m_0},$$

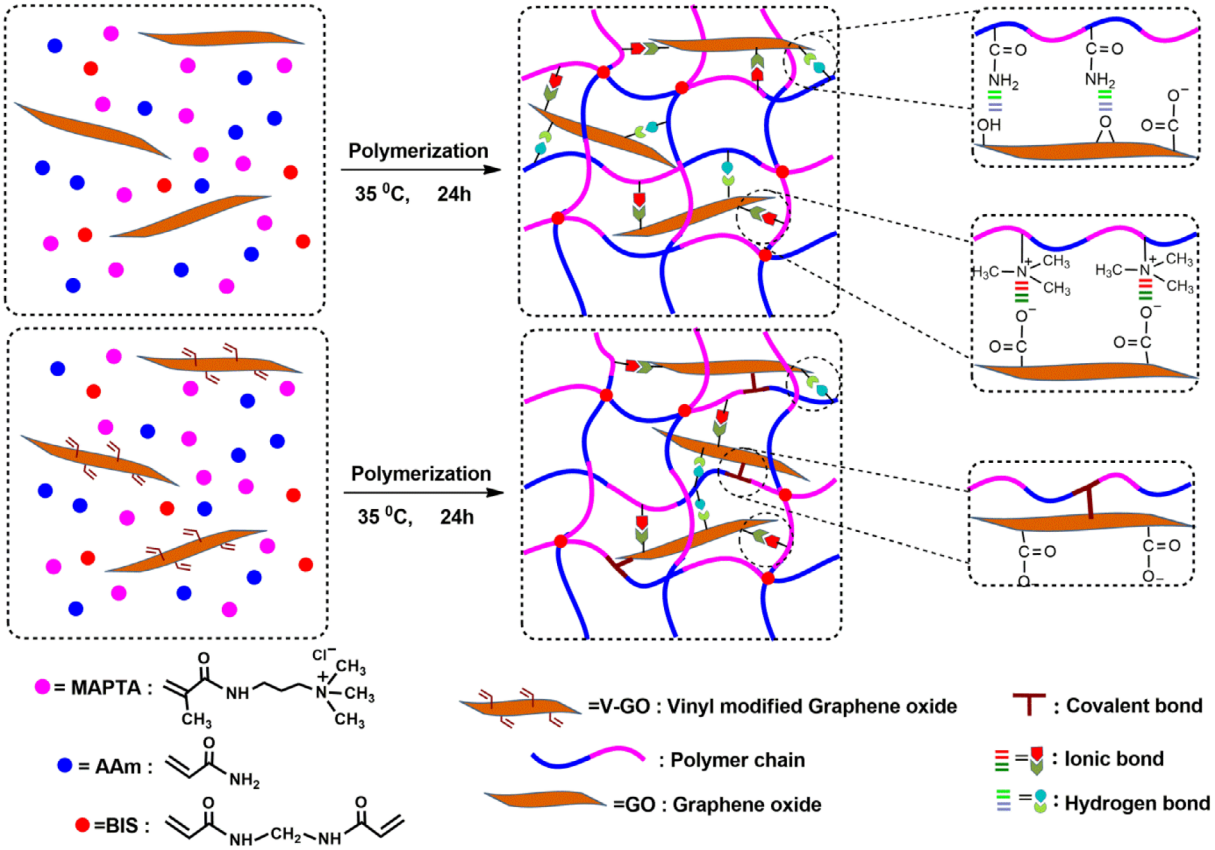

FIGURE 2 Schematic illustration of synthesis of GO and V-GO-based nanocomposite hydrogels

where m_0 and m are the dry and swollen weights of the gels at a given swelling time, respectively.

2.6 | Rheological measurements

A Bohlin Gemini 150 Rheometer system (Malvern Instruments, UK) was used to monitor gelation reactions and to examine viscoelastic properties of the final gels. The instrument was equipped with a Peltier device for temperature control and a cone-and-plate geometry (the cone is 40 mm in diameter, with a cone angle of 4°, and a truncation of 150 μm). In addition, a solvent trap was installed in the rheometer to prevent water evaporation during all rheological measurements. The polymerization solutions containing AAm (8.6 wt %), MAPTA (13.5 wt %), 0.029 wt % cross-linker (BIS) and initiator systems (APS, AIBA, ALD) were transferred between the rheometer plates, gelation reactions were carried out in the linear regime of oscillating deformation (deformation amplitude, $\gamma_o = 0.01$) and at a fixed angular frequency ($\omega = 6.28$ rad s^{-1}) at 35°C. Frequency-sweep tests were carried out at 25°C over the frequency range 3×10^{-1}–3×10^{2} rad s^{-1} at $\gamma_o = 0.01$.

2.7 | Mechanical tests

Prior to the mechanical tests, the water content of the hydrogels was adjusted to 30 wt% by controlled drying of the as-prepared gel specimens with a diameter of ~2.7 mm in sealed 50 ml vials at 23 ± 2°C in order to eliminate the water inside the gel to a suitable amount. This method was used to homogenize the gel specimens. The tensile tests were carried out by Zwick Roell test machine with a 500 N load cell and at a constant cross-head speed of 50 mm min^{-1}. The distance between the jaws was set to 10 ± 1 mm. Load and displacement data were collected during the experiments. The Young's modulus E was calculated from the slope of 5 and 15% deformation zone of stress–strain curves. Cyclic tensile experiments were performed at a strain rate of 5 min^{-1} to a maximum strain ε_{max} of 500%, followed by one-minute wait times between cycles.

2.8 | Testing self-healing efficiency

The self-healing efficiency of the hydrogels was determined by cut and-heal tests on gel samples with cylindrical forms of 2.7 mm in diameter, 1 cm in length and water content with 30%. The specimens were cut into middle and then two part of the gel were merged together from the fracture surfaces by slightly pressing. Distilled water was dropped to the cut surfaces and the water content of gels were balanced at 30% at room temperature for 24 h. Quantitative analysis of the healing efficiency of hydrogels was figured out from the ratios of Young's modulus E, fracture stress σ_f and elongation at

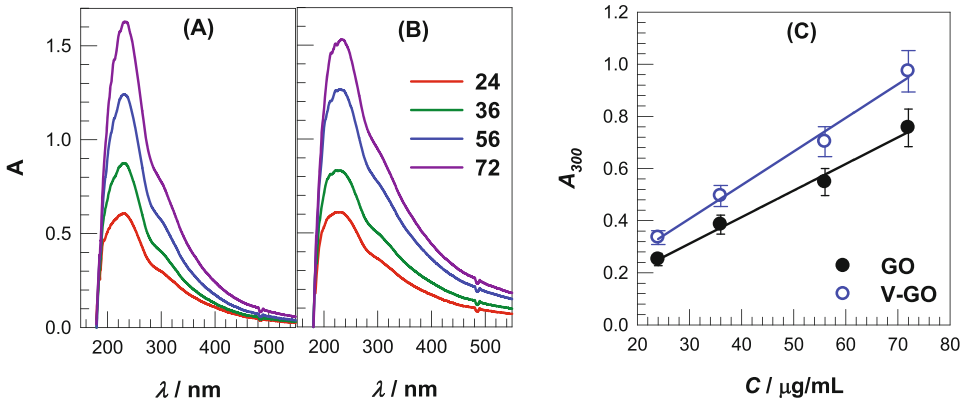

FIGURE 3 (A, B) UV–vis spectra of GO (A) and V-GO (B) at various concentrations in aqueous solution. The inset in (B) represent the nanosheet concentration in μg ml^{-1}. (C) Absorbance at 300 nm, A_{300}, plotted against the nanosheet concentration *C*

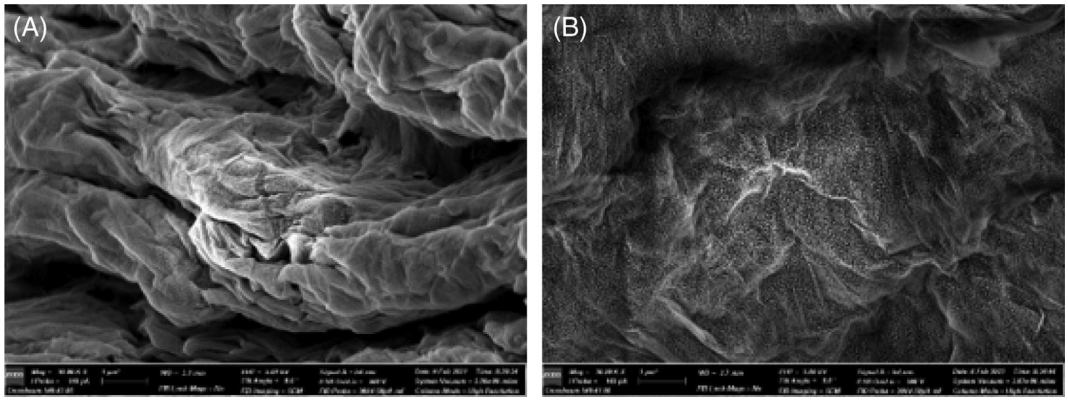

FIGURE 4 Field emission scanning electron microscope (FE-SEM) images of GO (A) and V-GO (B)

break ϵ_f of the healed samples by comparing with those of the virgin ones.

3 | RESULTS AND DISCUSSION

3.1 | Structural and morphological characterization of nanosheets and hydrogels

Figure 3 shows UV–vis absorption spectra of GO (a) and V-GO nanosheets (b) in aqueous dispersions prepared by ultrasonically dispersing. The spectra were recorded at various nanosheet concentrations between 24 and 72 μg ml^{-1} as indicated. An intense absorption peak at 232 nm belonging to the $\pi \rightarrow \pi^*$ transitions of the C=C bond and a less obvious peak at 300 nm, which is attributed to the $n \rightarrow \pi^*$ transitions of the C=O bond, are seen in the spectrum of GO.[55] After modification of GO with MPTS molecules to produce V-GO, the peak at 232 nm slightly shifts to 235 nm indicating formation of methacrylated GO nanosheets (Figure S3). The absorbance of both of GO and V-GO nanosheets at 300 nm increases linearly with their concentrations within the range of investigated (Figure 3C).

Field emission scanning electron microscopy (FE-SEM) was applied for investigating the morphology and uniformity of GO and V-GO nanosheets. As shown in Figure 4, GO nanosheets exhibit a rather rough and puffy morphology with a layer like structure,[56] while V-GO nanosheets display a rather smooth, flake-like microstructure, indicating change in the topography of GO after the silanization with MPTS. The results of DLS measurements revealed that the diameter at the peak of the size distribution is 1264 nm (89%), and 579 nm (80%), for GO and V-GO, respectively (Figure S4). The smaller size of V-GO compared to GO reveals disintegration of GO into smaller particles during the silanization reaction with MPTS.

FT-IR analysis was performed for GO and V-GO nanosheets as well as nanocomposite hydrogels. Figure 5A shows that the characteristic broad and intense peak of GO centered at 3316–3220 cm^{-1} due to hydroxyl groups is greatly decreased in the spectrum of V-GO due to the reaction of these groups with MPTS. The peaks at 2928 and 2896 cm^{-1} corresponding to symmetric and asymmetric vibrations of $-CH_3$ and $-CH_2-$ groups appearing in V-GO are assigned to the alkyl chains of its silane moieties.[57] The peak appearing at 1712 cm^{-1} is distinctive band of the C=O stretching mode of both carbonyl and ester groups. This peak becomes intense for V-GO due to the conjugation of methacrylate groups on GO by reaction with MPTS.[35,58] Moreover, the characteristic peak for vinyl group (C=C) at 1640 cm^{-1} after silanization was not clearly distinguished with the feature band at 1634 cm^{-1} due to the aromatic carbon structure (C=C) of GO nanosheet.[59] The band at 1377 cm^{-1}, which is attributed to stretching vibration of C–O of the hydroxyl group, almost disappeared after modification of V-GO.[60] The peak at 1296 cm^{-1} in the spectrum of V-GO is specified as stretching vibration of C–Si group of MPTS. The

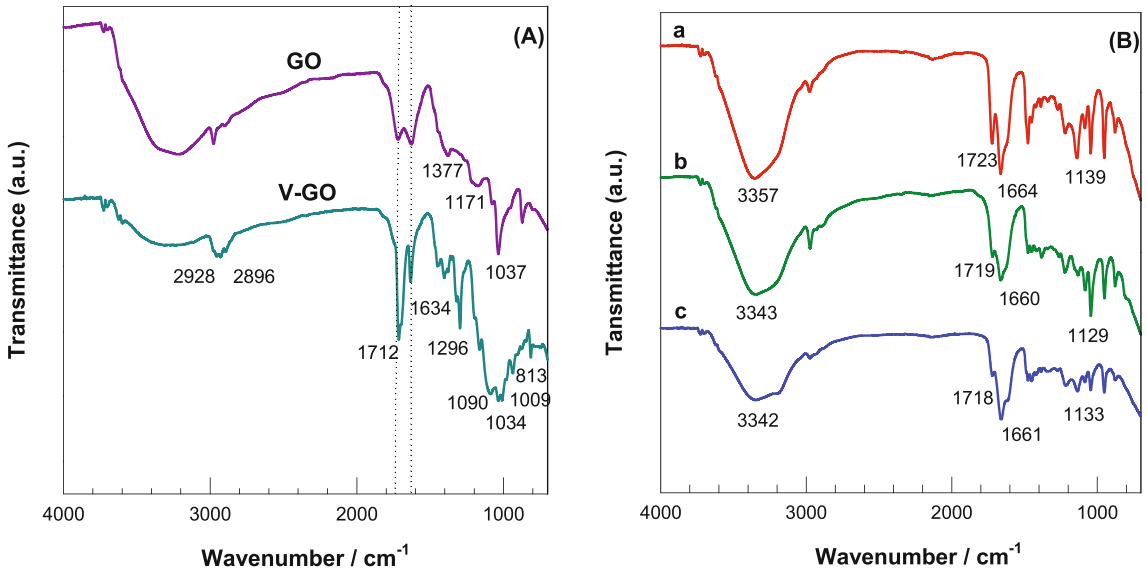

FIGURE 5 (A) FT-IR spectra of GO and V-GO, (B) FT-IR spectra of AAm-MAPTAC (A), AAm-MAPTAC/GO (B) and AAm-MAPTAC/V-GO hydrogels (C)

band at 1183 cm^{-1} is designated to stretching and bending vibrations of C–O of the epoxy group on GO. The appearance of characteristic vibrational spectral peak at 1090 cm^{-1} indicates the formation of siloxyl (Si–O) group, revealing the silanization of GO sheet. The peak at 1037 cm^{-1} is due to the stretching vibration of C–O group on GO nanosheets.[61]

FT-IR spectroscopy for hydrogels was carried out to elucidate the existence of two kinds of interactions due to hydrogen bonding between the amino group of AAm and the oxygen-containing group of GO, and electrostatic interaction between the quaternary ammonium group of MAPTAC and carboxyl group of GO. Figure 5B shows FT-IR spectra of the neat hydrogel (a), and nanocomposite hydrogels containing GO (b), and V-GO (c). It is seen that, after incorporation of GO and V-GO nanosheets into the hydrogel network, the band at 3357 cm^{-1} due to the characteristic N − H stretching of MAPTAC in the neat gel shifts to 3342 and 3343 cm^{-1} in gels containing GO and V-GO, respectively. Moreover, the typical C═O stretching of the $-CONH_2$ group of AAm in the neat gel shifts from 1723 cm^{-1} to 1719 and 1718 cm^{-1} in the presence of GO and V-GO, respectively. These shifts fully indicate the existence of hydrogen-bonding interactions between the amino groups of PAAm chains and GO nanosheets.[43,62,63] Additionally, a sharp absorbance at 1664 cm^{-1}, which is attributed to the carbonyl group (–CONH–) of the MAPTAC unit, is shifted to 1661 and 1660 cm^{-1} for hydrogels containing GO and V-GO, respectively, indicating formation of ionic bonds between the nanosheets and the polymer chains.[53]

Thermogravimetric analysis (TGA) was employed to elucidate the impact of silane functionalization and molecular changes in GO nanoparticles depending on chemical treatment (Figure S5). The TGA comparison between GO and V-GO showed that the mass loss from room temperature to 100°C is due to the loss of water molecules existing both on the surface and dominating in materials. The TGA curve for GO displayed a poor thermal stability with distinctive weight losses between 180 and 250°C due to the higher amounts of oxygen-containing functional groups. However, pronounced weight loss was observed between 250 and 300°C for V-GO. On the other hand, the remaining weight in the V-GO at temperatures higher than 400°C was 8%, whereas GO was entirely decomposed. All these TGA results revealed that the thermal stability of the V-GO was distinctly improved as a consequences of silane modification.[64]

3.2 | Swelling kinetics

The swelling tests are employed to understand the effect of GO and V-GO nanosheets on the extent of physical interactions in nanocomposite hydrogels. The tests were conducted at 23°C by immersing dried hydrogel specimens into water at acidic, neutral, and basic pH values. Figure 6 shows the swelling ratio m_{rel} of nanocomposite hydrogels containing GO (A, upper panel), and V-GO nanosheets (B, bottom panel) in water at pH = 3.0, 7.0, and 12 (from left to right) plotted against the swelling time. The black circles in the figures represent the data of the neat hydrogels. General trend is that, all hydrogels rapidly swell in water at pH = 3 and 7 until they attain their equilibrium states after a swelling time of around 1 day. A different behavior appears when they are immersed in water at pH 12; the mass of the hydrogels first increases within 1 day to attain a maximum degree of swelling while at longer times, they start to deswell and approach an equilibrium degree of swelling after 3 days. This swelling profile observed in both neat and nanocomposite hydrogels reveals that it is not specific for the nanosheets. One may explain this phenomenon with weaker electrostatic repulsions between ions in basic medium (pH 12) as compared to neural or acidic pH's because of the screening effect of hydroxyl ions, which increases the osmotic

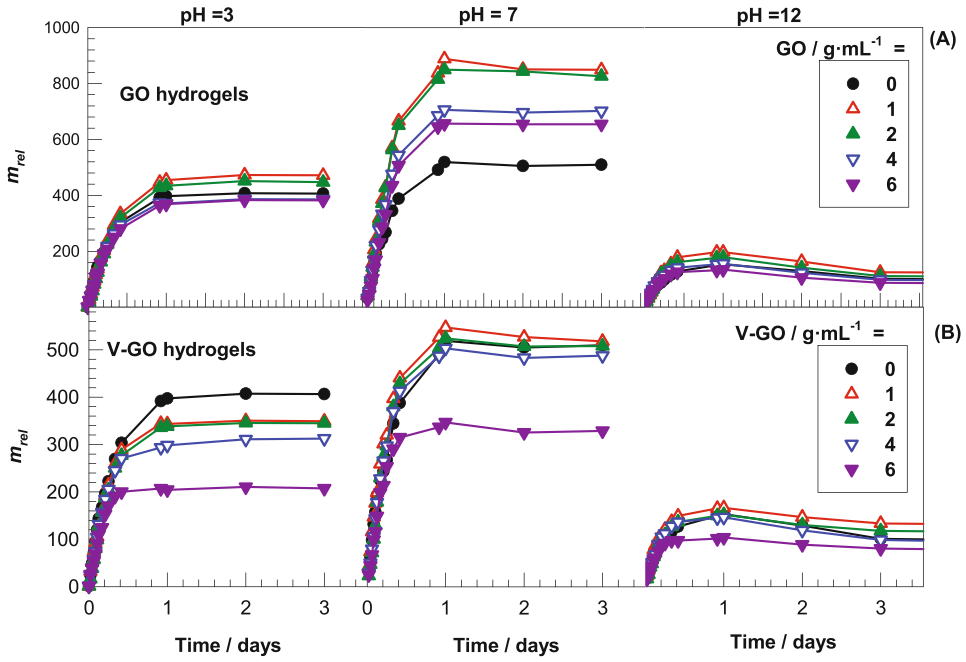

FIGURE 6 The swelling degrees m_{rel} of AAm-MAPTAC/GO (A) and AAm-MAPTAC/V-GO hydrogels (B) plotted against the time of swelling. pH = 3.0, 7.0, and 12 (from left to right). The amounts of GO and V-GO are indicated

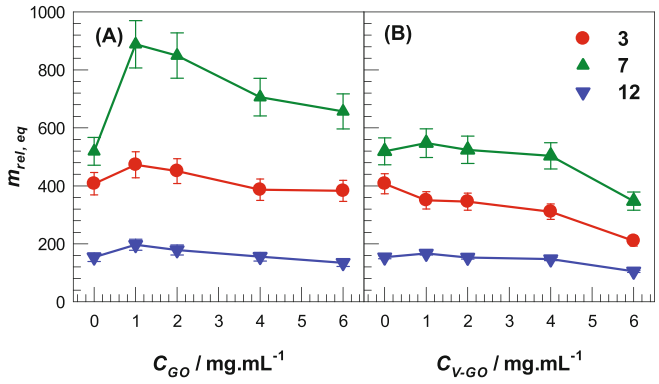

FIGURE 7 Equilibrium swelling degrees ($m_{rel,eq}$) of AAm-MAPTAC/GO (A) and AAm-MAPTAC/V-GO hydrogels (B) with various GO and V-GO loadings at pH 3.0 (red circles), pH 7.0 (green up triangles) and pH 12.0 (blue down triangles)

pressure in the medium leading to the decreasing swelling ratio of the hydrogels. In case of nanocomposite hydrogels, a partial release of GO from the hydrogels during the initial swelling process may also contribute to the gel deswelling at long swelling times due to the formation of carboxyl groups on GO at high pH values.

Figure 6A,B also shows that, although the initial swelling period of the neat and nanocomposite hydrogels is similar, their equilibrium degree of swelling depends on the type and amount of the nanosheets. To highlight this feature, the equilibrium swelling degrees ($m_{rel,eq}$) of all hydrogels are compiled in Figure 7A,B and plotted against their GO (A) and V-GO contents (B). The data are average of at least three measurements. It is seen that the swelling degree of GO-containing hydrogels is much higher than the neat ones at pH = 7 while this excess swelling decreases in acidic or basic pH's. This is attributed to the functional groups on the surface of GO nanosheets such as hydroxyl, epoxy, carbonyl, and carboxyl groups increasing the hydrophilicity of the nanocomposite gel. In addition, homogeneously dispersion of GO in the hydrogel as well as the synergetic intermolecular interactions between GO and polymer network might influence water retention property by increasing their swelling capacities. In contrast, $m_{rel,eq}$ of the hydrogels at a low or high pH is much lower which is attributed to the high concentration of ions in the solution leading to gel deswelling. Interestingly, replacing GO with V-GO nanosheets results in nanocomposite hydrogels with a lesser degree of swelling over all nanosheet concentration ranges (Figures 6B and 7B). This is attributed to the cross-linker effect of V-GO nanosheets chemically bonding to the network via their vinyl groups. Thus, the growing polymer radicals during the free radical copolymerization of AAm and MAPTAC may attack to the methacrylate groups on the V-GO surfaces to form chemical cross-links in addition to those formed by the BIS cross-linker.

3.3 | Rheological measurements

Formation of nanocomposite hydrogels was monitored by real-time dynamic rheological tests at a fixed angular frequency ($\omega = 6.28$ rad s^{-1}) and a strain amplitude of 1%. Figure 8 represents typical gelation profiles nanocomposite hydrogels containing various amounts of GO (upper panel) and V-GO nanosheets (bottom panel). In the figure, the storage modulus G' (filled blue circles), loss modulus G'' (open black triangles) and loss factor tan δ (curves) as a function of the reaction time are plotted. An induction period of around 20 min is seen in the gelation profile of the neat hydrogel while its duration shortened when the nanosheets are included into the reaction system. This shortening effect is more significant in the presence of GO, as better seen in Figure 9, showing semilogarithmic plots G' (symbols),

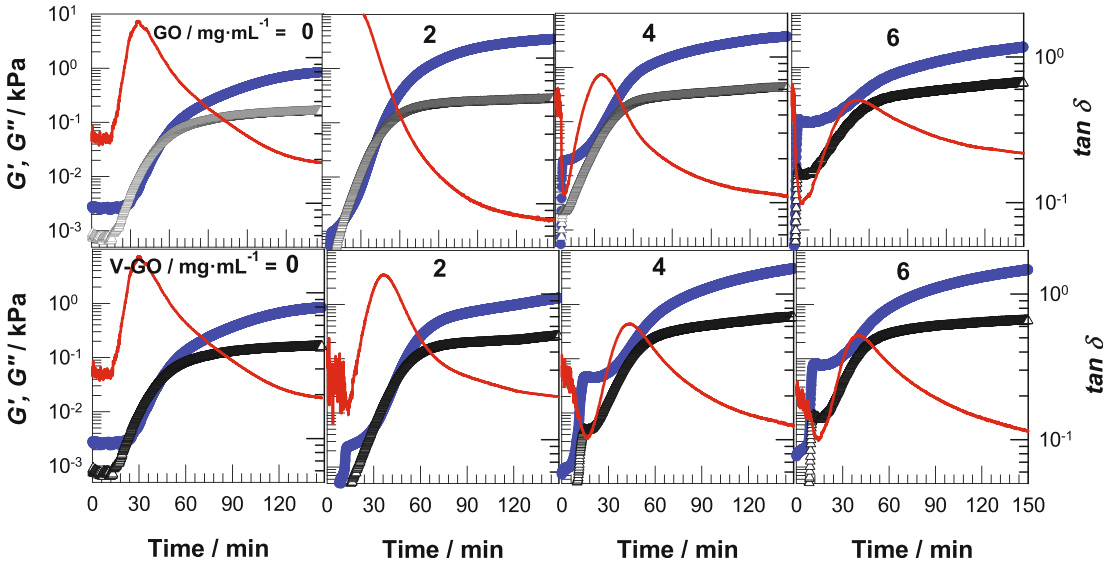

FIGURE 8 Storage modulus G' (filled symbols), the loss modulus G'' (open symbols), and loss factor tan δ (lines) during the polymerization of AAm-MAPTAC (22.1 wt %) with BIS (0.029 wt %) and GO (upper panel) or V-GO (bottom panel) at 35°C shown as a function of the reaction time. $\omega = 6.3$ rad s^{-1}, and $\gamma_0 = 0.01$

FIGURE 9 Semilogarithmic plots of G' (symbols), and tan δ (lines) during the polymerization of the hydrogels without and with 6 mg ml^{-1} GO and V-GO. The parameters are the same as in Figure 8

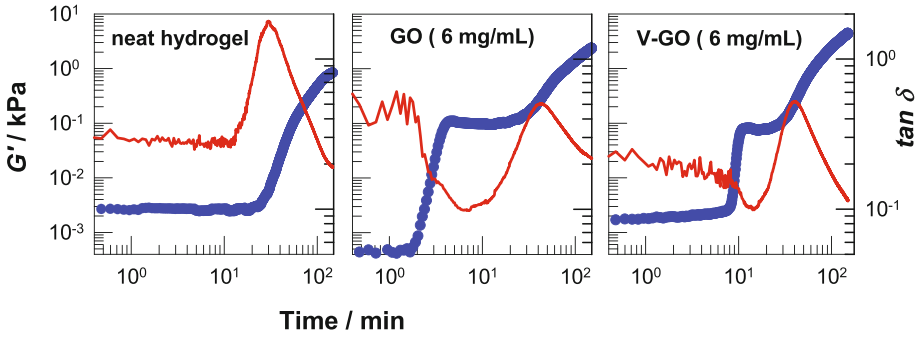

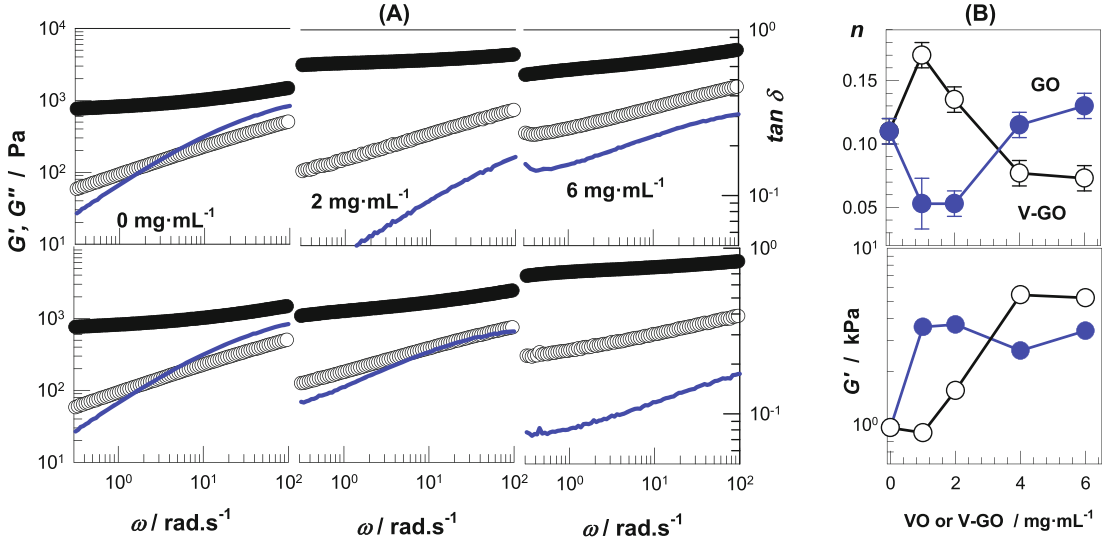

FIGURE 10 (A) Frequency dependence of G' (filled symbols), G'' (open symbols), and tan δ (curves) of nanocomposite hydrogels with GO (upper panel) and V-GO (bottom panel) after a reaction time of 150 min. Nanosheet contents as indicated. (B) The exponent n and the modulus G' at $\omega = 6.28$ rad s^{-1} both plotted against the nanosheet content

and tan δ (lines) during the gelation reactions without and with 6 mg ml^{-1} GO and V-GO (from left to right).

Another interesting feature of nanocomposite hydrogels is their two-step gelation profile which is not seen for the neat hydrogel (Figure 9); G' first abruptly increases while tan δ decreases within 5 min to attain a plateau value while at longer times G' starts to increase again to approach a second plateau. This finding indicates formation of two types of cross-links in nanocomposite hydrogels. Because the first step is absent in the neat hydrogel, the results suggest that this step is due to the nanoparticle-polymer interactions and reflects formation of dynamic cross-links between the growing polymer radicals and nanoparticles. Moreover, the second step of gelation is similar to the neat hydrogel and hence, corresponds to the formation of cross-links via BIS cross-linker.

Figure 10A shows the frequency dependences of G' (filled symbols), G'' (open symbols), and tan δ (curves) of nanocomposites hydrogels with GO (upper panel) and V-GO (bottom panel) after a reaction time of 150 min. Although the incorporation of the nanosheets into the gel network increases G' of nanocomposite hydrogels and hence increases their cross-link density, tan δ only slightly decreases and still remains at around 0.1. Because tan δ reflects the magnitude of the dissipated to stored energy under strain, nanocomposite hydrogels have also viscous character due to the nanoparticles dynamically interacting with the polymer chains. Moreover, G' of all hydrogels exhibits a power law dependence on the frequency, $G' \sim \omega^n$. In Figure 10B, the exponent n together the moduli G' of the hydrogels measured at $\omega = 6.28$ rad s^{-1} are plotted against the nanosheet contents. Interestingly, the type of the nanosheets affects oppositely on the value of both n and G' at concentrations below 4 mg ml^{-1}. Incorporation of GO decreases n, indicating decreasing frequency dependence and increasing lifetime of the cross-links while V-GO addition increases the frequency dependence and hence shorten the lifetime of cross-links. This finding reveals that the network chains interact more strongly with GO rather than V-GO nanosheets, which is likely due to the presence of a larger number of hydrophilic groups on the surfaces of GO as compared to V-GO. However, as the nanosheet content is increased above 4 mg ml^{-1}, V-GO produces hydrogels with a higher modulus and longer lifetimes as compared to GO due to the formation of chemical cross-links between the polymer chains and V-GO nanosheets via their surface vinyl groups.

3.4 | Mechanical properties and healing behavior of nanocomposite hydrogels

Uniaxial tensile tests were performed at 23 ± 2°C on hydrogels formed after a reaction time of 24 h. It should be noted that the tests are conducted on hydrogels containing 30 wt % water because, in their as-prepared states with 70 wt % water, they were too weak to distinguish the effect of nanosheets on the mechanical properties of hydrogels (Figure S6). Figure 11A,B shows tensile stress–strain curves of nanocomposite hydrogels containing various amounts of GO (A) and V-GO nanosheets (B). The data of the neat hydrogel in both

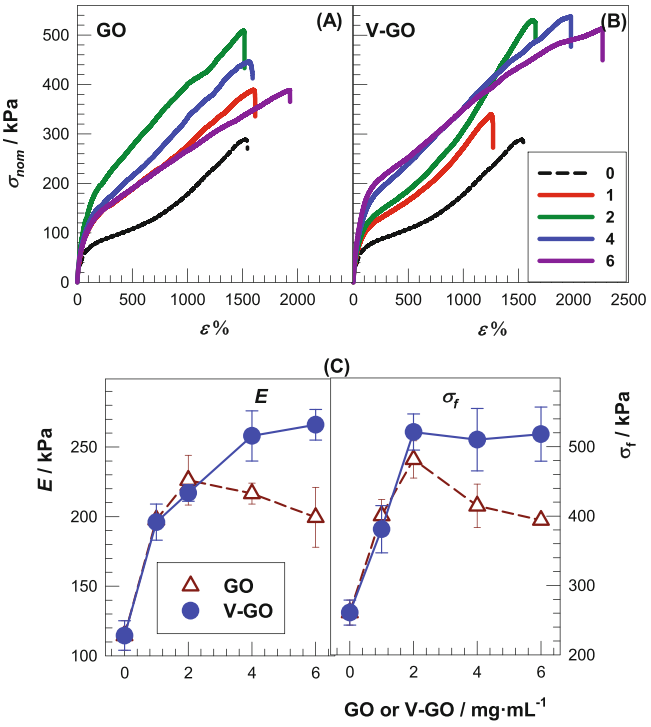

FIGURE 11 (A, B) Tensile stress–strain curves of nanocomposite hydrogels prepared in the presence of GO (A) and V-GO (B) as the dependence of the nominal stress σ_{nom} on the deformation ratio ϵ. $\dot{\varepsilon} = 1$ min^{-1}. (C) Young's modulus E and fracture stress σ_f of the hydrogels plotted against the nanosheet content

graphs are shown by the black dashed curves. The incorporation of GO does not change much the high stretchability of the neat hydrogel of around 1500%. In contrast, incorporation of V-GO increases the stretchability up to 2200% at its highest amount of 6 mg ml^{-1}. Moreover, Young's modulus E and the fracture stress σ_f of the hydrogels summarized in Figure 11C reveal increasing modulus and strength of the neat hydrogel upon incorporation of the nanosheets. The effects of GO and V-GO on the enhancement in the mechanical properties are similar up to a nanosheet content of 2 mg ml^{-1}. For instance, the modulus increases from 115 ± 11 to around 220 kPa for both nanosheets revealing additional cross-links formation due to the polymer-nanoparticle interactions. However, at higher concentrations, increasing amount of GO leads to a decrease in the modulus while V-GO addition further increases the modulus up to 266 ± 10 kPa at 6 mg ml^{-1}. This highlights the formation of additional cross-links by means of methacrylate groups bound to V-GO nanosheets that act as a multifunctional cross-linker. Moreover, the nanosheets also induce a significant enhancement in the fracture stress of the hydrogels the extent of which is larger when V-GO instead of GO was used in the gel preparation.

Besides that the improvement in strength and modulus, AAm-MAPTAC hydrogels with or without nanosheets also exhibited good recovery properties. The stress–strain curves of the cyclic tests for the hydrogels with and without nanosheets were examined by conducting five successive loading/unloading cycles at a fixed duration of

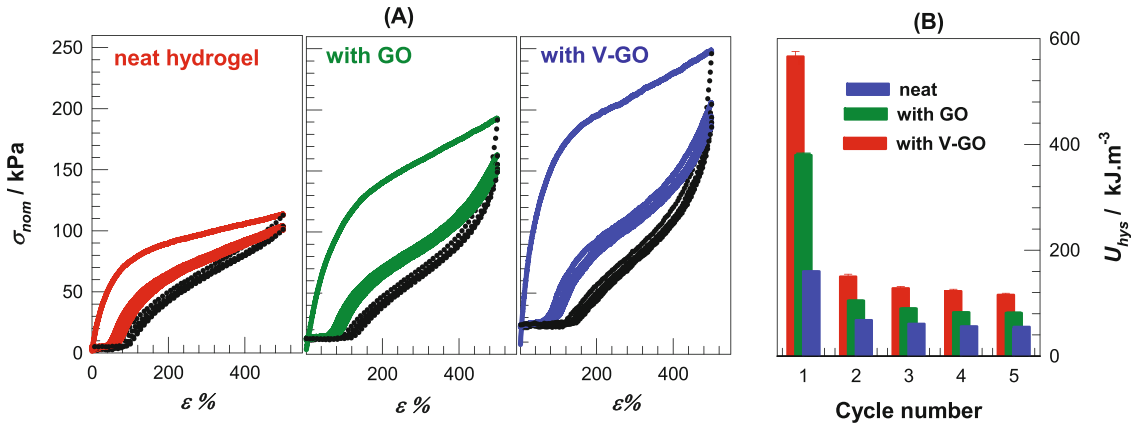

FIGURE 12 (A) Five successive cyclic tensile test results conducted on the neat hydrogel and nanocomposite hydrogels with GO and V-GO at a concentration of 6 mg ml^{-1}. Loading and unloading steps are shown by solid and dotted black curves, respectively. Waiting time between cycles is 1 min. (B) Hysteresis energies U_{hys} of the hydrogels calculated from the tensile cycles in (A) plotted against the cycle number

1 min between the cycles (Figure 12A). The hysteresis energy U_{hys}, that is, the area enclosed by the tensile cycle is shown in Figure 12B plotted against the cycle numbers.

It is noteworthy that the loading and unloading steps are different in the graphs due to the damage formed in hydrogel. Moreover, both the neat and nanocomposite hydrogels exhibit a large mechanical hysteresis during the 1st cycle while it significantly decreases in the following cycles. The hysteresis energy U_{hys} of the 1st cycle is 160, 380, and 565 kJ m^{-3} for the neat hydrogel, GO- and V-GO-containing hydrogels, respectively. The same trend is seen for the following cycles reflecting existence of the largest number of intermolecular bonds in hydrogels containing V-GO nanosheets. It is also noticeable that all cycles after the 1st one exhibit reversible behavior with a constant hysteresis energy indicating reversible breakage and reformation of bonds. From these results, we can conclude that the covalent bonds in the hydrogels are broken irreversibly during the 1st cycle while during the following cycles, the physical bonds between the polymer chains and nanosheets break and reform reversibly. The number of both types of bonds increases in order of neat hydrogel <GO containing hydrogel <V-GO containing hydrogels. This highlights the effect of surface methacrylate groups on V-GO on the microstructure of the hydrogels. The existence of physical bonds and their recoverability upon unloading predict self-healing behavior of the hydrogels with or without nanosheets. This was indeed observed experimentally.

For the healing tests, the hydrogel samples with a cylindrical shape were first cut into half, and the cut surfaces were pressed together by hand at room temperature (23 ± 2°C) to induce an autonomic healing (Figure S7). Preliminary experiments showed that an efficient healing can be generated when water was used as a healing agent, as reported before for GO-containing hydrogels based on AAm and DAC.[51] The images in Figure 13 shows a gel sample after cutting (a), adding one drop of water on the combined cut area (b), and sixfold stretching of the healed sample after a healing time of 24 h at room temperature.

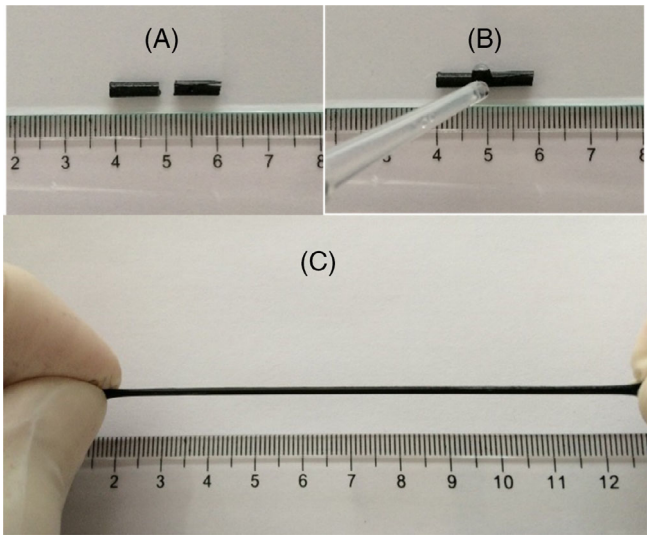

FIGURE 13 Self-healing behavior **o**f the hydrogels. After cutting into two parts (A), and dropping water on the combined cut area results in healing of both neat and nanocomposite hydrogels (B, C)

Figure 14A,B shows stress–strain curves of virgin (solid curves) and healed hydrogels (dashed curves) containing GO and V-GO, respectively, at various concentrations. It is seen that the initial part of the curves for the healed samples closely follows those of the virgin ones. Indeed, the healing efficiency of all hydrogels with respect to the modulus E was 98 ± 4% indicating the recovery of the original microstructure. In Figure 14C, the healing efficiencies of GO- and V-GO-containing hydrogels with respect to the fracture strain ϵ_f, and fracture stress σ_f are plotted against the nanosheet concentration. Note that the data at zero concentration corresponds to the neat hydrogels. The general trend is that the incorporation of the nanosheets decreases the self-healing efficiency of the hydrogels with respect to their ultimate mechanical properties, and this decrease is more significant for V-GO-containing hydrogels. This behavior is associated with the reduction in flexibility of polymer

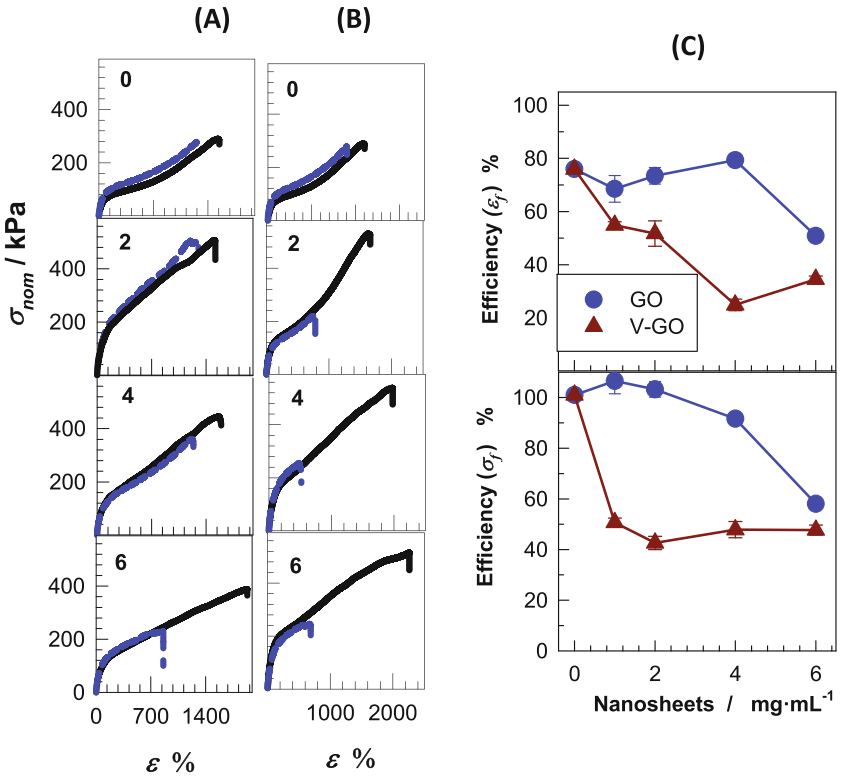

FIGURE 14 (A, B) Stress–strain curves of virgin (solid black curves) and healed hydrogels (dashed blue curves) containing GO (A) and V-GO (B) at various concentrations as indicated in mg ml^{-1}. (C) The healing efficiencies with respect to strain at break ϵ_f, and fracture stress σ_f of GO and V-GO containing hydrogels plotted against the nanosheet content

chains because of the interactions between GO or V-GO and the polymer network. On the other hand, the lowest healing efficiency of V-GO-containing hydrogels is due to the chemical cross-links between the polymer chains and V-GO nanoparticles via their pendant methacrylate groups.

4 | CONCLUSION

In summary, we have demonstrated and compared the improvement in the mechanical performance and self-healing ability of nanocomposite cationic hydrogels prepared with GO and V-GO nanosheets bound to the polymer network by physical interactions and chemical cross-links, respectively. AAm-MAPTAC hydrogels with V-GO exhibit lower equilibrium swelling degree in each pH solution than that those prepared with GO, indicating that chemically binding of the nanosheets to the network structure discloses a multifunctional cross-linker behavior of V-GO. High stretching ability (up to 2200%), Young's modulus (up to 260 kPa) and a tensile strength up to 520 kPa were obtained for AAm-MAPTAC hydrogels with V-GO. Tensile tests revealed that increase in content of nanosheets remarkably enhanced both the modulus and the fracture stress of the hydrogels, while elongation at break remained almost the same. Compared to the neat AAm-MAPTAC hydrogels, 3-fold increase in Young's modulus and 2-fold increase in fracture stress were obtained for AAm-MAPTAC hydrogels containing a high amount of V-GO nanosheets. The analysis of self-healing properties of nanocomposite gels disclosed that the modulus-dependent self-healing efficiency of all hydrogels was around 100%, whereas the healing performance with respect to the ultimate mechanical properties decreases with increasing GO content, and this decrease is more significant for V-GO nanosheets. The results reveal that nanosheets bounded chemically to hydrogel provide enhancing stability and durability because of homogeneous distribution of nanoparticles in the network, which may have been crucial in the inception and sustainability of gel applications.

ACKNOWLEDGMENTS

The authors thank Istanbul Technical University (BAP Project number: 42666) for their financial support.

CONFLICT OF INTEREST

The authors declare no potential conflict of interest.

DATA AVAILABILITY STATEMENT

The data that support the findings of this study are available from the corresponding author upon reasonable request.

ORCID

Ezgi B. Çeper https://orcid.org/0000-0002-2595-9846
Oguz Okay https://orcid.org/0000-0003-2717-4150

REFERENCES

1. Blaiszik BJ, Kramer SLB, Olugebefola SC, Moore JS, Sottos NR, White SR. Self-healing polymers and composites. *Annu Rev Mat Res*. 2010;40:179-211.
2. Liu Y, Hsu SH. Synthesis and biomedical applications of self-healing hydrogels. *Front Chem*. 2018;6:449.
3. Taylor DL, In Het Panhuis M. Self-healing hydrogels. *Adv Mater*. 2016; 28:9060-9093.

4. Jiang H, Duan L, Ren X, Gao G. Hydrophobic association hydrogels with excellent mechanical and self-healing properties. *Eur Polym J*. 2019;112:660-669.
5. Okay O. Self-healing hydrogels formed via hydrophobic interactions. *Supramolecular Polymer Networks and Gels*. Springer International Publishing; 2015:101.
6. Gong Z, Zhang G, Zeng X, et al. High-strength, tough, fatigue resistant, and self-healing hydrogel based on dual physically cross-linked network. *ACS Appl Mater Interfaces*. 2016;8:24030-24037.
7. Ding Q, Xu X, Yue Y, et al. Nanocellulose-mediated electroconductive self-healing hydrogels with high strength, plasticity, viscoelasticity, Stretchability, and biocompatibility toward multifunctional applications. *ACS Appl Mater Interfaces*. 2018;10:27987-28002.
8. Shi L, Ding P, Wang Y, Zhang Y, Ossipov D, Hilborn J. Self-healing polymeric hydrogel formed by metal-ligand coordination assembly: design, fabrication, and biomedical applications. *Macromol Rapid Commun*. 2019;40:1800837.
9. Mozhdehi D, Ayala S, Cromwell OR, Guan Z. Self-healing multiphase polymers via dynamic metal-ligand interactions. *J Am Chem Soc*. 2014;136(46):16128-16131.
10. Liang Y, Zhao X, Hu T, et al. Adhesive hemostatic conducting injectable composite hydrogels with sustained drug release and photothermal antibacterial activity to promote full-thickness skin regeneration during wound healing. *Small*. 2019;15(12):1900046.
11. Yang B, Song J, Jiang Y, et al. Injectable adhesive self-healing multicross-linked double-network hydrogel facilitates full-thickness skin wound healing. *ACS Appl Mater Interfaces*. 2020;12(52):57782-57797.
12. Guo Y, Zhou X, Tang Q, Bao H, Wang G, Saha PA. Self-healable and easily recyclable supramolecular hydrogel electrolyte for flexible supercapacitors. *J Mater Chem A*. 2016;4(22):8769-8776.
13. Li X, Yang Q, Zhao Y, Long S, Zheng J. Dual physically crosslinked double network hydrogels with high toughness and self-healing properties. *Soft Matter*. 2017;13(5):911-920.
14. Yu H, Wang Y, Yang H, Peng K, Zhang X. Injectable self-healing hydrogels formed via thiol/disulfide exchange of thiol functionalized F127 and dithiolane modified PEG. *J Mater Chem B*. 2017;5(22):4121-4127.
15. Li Y, Yang L, Zeng Y, Wu Y, Wei Y, Tao L. Self-healing hydrogel with a double dynamic network comprising imine and borate Ester linkages. *Chem Mater*. 2019;31(15):5576-5583.
16. Shao C, Wang M, Chang H, Xu F, Yang JA. Self-healing cellulose nanocrystal-poly(ethylene glycol) nanocomposite hydrogel via Diels–Alder click reaction. *ACS Sustain Chem Eng*. 2017;5(7):6167-6174.
17. Deng G, Li F, Yu H, et al. Dynamic hydrogels with an environmental adaptive self-healing ability and dual responsive sol–gel transitions. *ACS Macro Lett*. 2012;1(2):275-279.
18. He L, Fullenkamp DE, Rivera JG, Messersmith PB. pH responsive self-healing hydrogels formed by boronate-catechol complexation. *Chem Comm*. 2011;47(26):7497-7499.
19. Li W, Lu S, Zhao M, et al. Self-healing cellulose Nanocrystals-containing gels via reshuffling of Thiuram disulfide bonds. *Polymers*. 2018;10(12):3390.
20. Fan L, Ge X, Qian Y, et al. Advances in synthesis and applications of self-healing hydrogels. *Front Bioeng Biotechnol*. 2020;8:654.
21. Liu Y, He W, Zhang Z, Lee BP. Recent developments in tough hydrogels for biomedical applications. *Gels*. 2018;4(2):3390.
22. Chen Q, Chen H, Zhu L, Zheng J. Fundamentals of double network hydrogels. *J Mater Chem B*. 2015;3(18):3654-3676.
23. Nakajima T, Gong JP. Double-network hydrogels: soft and tough IPN. *Encyclopedia of Polymeric Nanomaterials*. Springer; 2013:1.
24. Okumura YKI. The Polyrotaxane gel: a topological gel by figure-of-eight cross-links. *Adv Mater*. 2001;13(7):485-487.
25. Murakami T, Schmidt BVKJ, Brown HR, Hawker CJ. One-pot "click" fabrication of slide-ring gels. *Macromolecules*. 2015;48(21):7774-7781.
26. Dannert C, Stokke BT, Dias RS. Nanoparticle-hydrogel composites: from molecular interactions to macroscopic behavior. *Polymers*. 2019;11(2):275.
27. Thoniyot P, Tan MJ, Karim AA, Young DJ, Loh XJ. Nanoparticle-hydrogel composites: concept, design, and applications of these promising, multi-functional materials. *Adv Sci*. 2015;2:1-13.
28. Uzumcu AT, Guney O, Okay O. Nanocomposite DNA hydrogels with temperature sensitivity. *Polymer*. 2016;100:169-178.
29. Pan C, Liu L, Gai G. Recent progress of graphene-containing polymer hydrogels: preparations, properties, and applications. *Macromol Mater Eng*. 2017;302(10):1-14.
30. Gupta T, Pradhan A, Bandyopadhyay-Ghosh S, Ghosh SB. Thermally exfoliated graphene oxide reinforced stress responsive conductive nanocomposite hydrogel. *Polym Adv Technol*. 2019;30(9):2392-2401.
31. Farjadian F, Abbaspour S, Sadatlu MAA, et al. Recent developments in graphene and graphene oxide: properties, synthesis, and modifications: a review. *Chem Select*. 2020;5(33):10200-10219.
32. Smith AT, LaChance AM, Zeng S, Liu B, Sun L. Synthesis, properties, and applications of graphene oxide/reduced graphene oxide and their nanocomposites. *Nano Mater Sci*. 2019;1(1):31-47.
33. Rohani Rad E, Vahabi H, Formela K, Saeb MR, Thomas SJ. Injectable poloxamer/graphene oxide hydrogels with well-controlled mechanical and rheological properties. *Polym Adv Technol*. 2019;30(9):2250-2260.
34. Feicht P, Biskupek J, Gorelik TE, et al. Brodie's or Hummers' method: oxidation conditions determine the structure of graphene oxide. *Chemistry*. 2019;25(38):8955-8959.
35. Yu H, Zhang B, Bulin C, Li R, Xing R. High-efficient synthesis of graphene oxide based on improved hummers method. *Sci Rep*. 2016;6:36143.
36. Cheng H, Huang Y, Cheng Q, Shi G, Jiang L, Qu L. Self-healing graphene oxide based functional architectures triggered by moisture. *Adv Funct Mater*. 2017;27:1703096.
37. Jo H, Sim M, Kim S, et al. Electrically conductive graphene/polyacrylamide hydrogels produced by mild chemical reduction for enhanced myoblast growth and differentiation. *Acta Biomater*. 2017;48:100-109.
38. Cheng Y, Ren K, Huang C, Wei J. Self-healing graphene oxide-based nanocomposite hydrogels serve as near-infrared light-driven valves. *Sens Actuators B Chem*. 2019;298:126908.
39. Liu J, Song G, He C, Wang H. Self-healing in tough graphene oxide composite hydrogels. *Macromol Rapid Commun*. 2013;34(12):1002-1007.
40. Li G, Xiao P, Hou S, Huang Y. Graphene based self-healing materials. *Carbon*. 2019;146:371-387.
41. Uzumcu AT, Guney O, Okay O. Highly stretchable DNA/clay hydrogels with self-healing ability. *ACS Appl Mater Interfaces*. 2018;10(9):8296-8306.
42. Peng S, Zhang D, Huang H, Jin Z, Peng X. Ionic polyacrylamide hydrogel improved by graphene oxide for efficient adsorption of methylene blue. *Res Chem Intermed*. 2018;45(3):1545-1563.
43. Cui W, Ji J, Cai YF, Li H, Ran RJ. Robust, anti-fatigue, and self-healing graphene oxide/hydrophobically associated composite hydrogels and their use as recyclable adsorbents for dye wastewater treatment. *J Mater Chem A*. 2015;3(33):17445-17458.
44. Saya L, Gautam D, Malik V, Singh WR, Hooda S. Natural polysaccharide based graphene oxide nanocomposites for removal of dyes from wastewater: a review. *J Chem Eng Data*. 2020;66(1):11-37.
45. Huang Y, Wang C, Shao C, et al. Graphene oxide assemblies for sustainable clean-water harvesting and green-electricity generation. *Acc Mater Res*. 2021;2(2):97-107.
46. Oh JS, Lee EJ. Photodynamic graphene oxide combined alginate hydrogel for controlled drug release. *Macromol Res*. 2021;29(5):383-390.

47. Olate MF, Palza HJ. Effect of graphene oxide on the pH-responsive drug release from supramolecular hydrogels. *J Appl Polym Sci*. 2022; 139:e51420.
48. Wang T, Huang J, Yang Y, Zhang E, Sun W, Tong Z. Bioinspired smart actuator based on graphene oxide-polymer hybrid hydrogels. *ACS Appl Mater Interfaces*. 2015;7(42):23423-23430.
49. Wang Y, Chang Q, Zhan R, et al. Tough but self-healing and 3D printable hydrogels for E-skin, E-noses and laser controlled actuators. *J Mater Chem A*. 2019;7(43):24814-24829.
50. Kolanthai E, Sindu PA, Khajuria DK, et al. Graphene oxide-a tool for the preparation of chemically crosslinking free alginate-chitosan-collagen scaffolds for bone tissue engineering. *ACS Appl Mater Interfaces*. 2018;10(15):12441-12452.
51. Liu X, Miller AL, Waletzki BE, Lu L. Cross-linkable graphene oxide embedded nanocomposite hydrogel with enhanced mechanics and cytocompatibility for tissue engineering. *J Biomed Mater Res A*. 2018; 106(5):1247-1257.
52. Shen J, Yan B, Li T, Long Y, Li N, Ye M. Mechanical, thermal and swelling properties of poly(acrylic acid)–graphene oxide composite hydrogels. *Soft Matter*. 2012;8(6):1831-1836.
53. Pan C, Liu L, Chen Q, Zhang Q, Guo G. Tough, stretchable, compressive novel polymer/graphene oxide nanocomposite hydrogels with excellent self-healing performance. *ACS Appl Mater Interfaces*. 2017; 9(43):38052-38061.
54. Hu X, Su E, Zhu B, Jia J, Yao P, Bai Y. Preparation of silanized graphene/poly (methyl methacrylate) nanocomposites in situ copolymerization and its mechanical properties. *Compos Sci Technol*. 2014; 97:6-11.
55. Cha C, Shin SR, Gao X, et al. Controlling mechanical properties of cell-laden hydrogels by covalent incorporation of graphene oxide. *Small*. 2014;10(3):514-523.
56. Güney S, Arslan T, Yanık S, Güney O. An electrochemical sensing platform based on graphene oxide and molecularly imprinted polymer modified electrode for selective detection of amoxicillin. *Electroanalysis*. 2021;33(1):46-56.
57. Li W, Zhou B, Wang M, Li Z, Ren R. Silane functionalization of graphene oxide and its use as a reinforcement in bismaleimide composites. *J Mater Sci*. 2015;50(16):5402-5410.
58. Zhong M, Liu YT, Xie XM. Self-healable, super tough graphene oxide-poly(acrylic acid) nanocomposite hydrogels facilitated by dual cross-linking effects through dynamic ionic interactions. *J Mater Chem B*. 2015;3(19):4001-4008.
59. Chekin F, Bagheri S, Abd Hamid SB. Functionalization of graphene oxide with 3-mercaptopropyltrimethoxysilane and its electrocatalytic activity in aqueous medium. *J Chin Chem Soc*. 2015;62(8):689-694.
60. Fan J, Shi Z, Lian M, Li H, Yin J. Mechanically strong graphene oxide/sodium alginate/polyacrylamide nanocomposite hydrogel with improved dye adsorption capacity. *J Mater Chem A*. 2013;1(25):7433-7443.
61. Paredes JI, Villar-Rodil S, Martínez-Alonso A, Tascón JMD. Graphene oxide dispersions in organic solvents. *Langmuir*. 2008;24:10560-10564.
62. Liu R, Liang S, Tang XZ, Yan D, Li X, Yu ZZ. Tough and highly stretchable graphene oxide/polyacrylamide nanocomposite hydrogels. *J Mater Chem A*. 2012;22(28):14160-14167.
63. Cong HP, Wang P, Yu SH. Highly elastic and superstretchable graphene oxide/polyacrylamide hydrogels. *Small*. 2014;10(3): 448-453.
64. Paz E, Ballesteros Y, Forriol F, Dunne N, Del Real J. Graphene and graphene oxide functionalisation with silanes for advanced dispersion and reinforcement of PMMA-based bone cements. *Mater Sci Eng C*. 2019;104:109946.

SUPPORTING INFORMATION

Additional supporting information may be found in the online version of the article at the publisher's website.

How to cite this article: Çeper EB, Su E, Okay O, Güney O. Surface modification of graphene oxide for preparing self-healing nanocomposite hydrogels. *Polym Adv Technol*. 2022; 33(7):2276-2288. doi:10.1002/pat.5680